Multicycle Dynamics of Fault Systems and Static and Dynamic Triggering of Earthquakes

L.M. Olsen-Kettle[1], D. Weatherley, L. Gross and H.-B. Mühlhaus

Earth Systems Science Computational Centre, University of Queensland, Australia

[1] lkettle@esscc.uq.edu.au

ABSTRACT

Dynamic simulations of rupture propagation and multiple earthquake cycles for varying fault geometries are presented. We demonstrate the importance of the frictional law employed and mesh size dependence in obtaining a rich spectrum of event sizes over multiple earthquake cycles. We investigate the role of both dynamic and static stress changes on earthquake triggering in interacting two-fault models. Dynamic stress triggering of earthquakes is caused by the passage of seismic waves, whereas static stress triggering is due to net slippage on a fault resulting from an earthquake. Static stress changes represented by a Coulomb failure function and its relationship to seismicity rate change is a relatively well-known mechanism, whereas the physical origin of dynamic triggering remains one of the least understood aspects of earthquake nucleation. We investigate these mechanisms by analysing seismicity patterns with varying fault separation, geometry and with and without dynamic triggering present.

1 Elasto-plastic Fault Model

We study numerical solutions of the 2D wave equation:

$$\rho \ddot{u}_i(t) = \sigma_{ij,j} + F_i, \quad (1)$$

subject to boundary conditions:

$$\sigma_{ij} n_j = F_n n_j + F_\tau \tau_j \text{ on fault interfaces,} \quad (2)$$

where $\boldsymbol{u}$ is the displacement, ρ is the density, $\boldsymbol{F}$ is a body force, and σ is the stress tensor. $\boldsymbol{n}$ and $\boldsymbol{\tau}$ are the normal and tangential vectors at each fault respectively, and the tractions F_n and F_τ represent the normal and shear stress acting on the fault respectively and are given using the penalty method and elasto-plasticity theory. The fault contact elements are represented by zero-thickness joint elements where the displacements across the fault can be discontinuous and consist of an elastic plus a plastic component. The magnitude of the plastic component is given by the Coulomb failure function (CFF) and ensures that at all time the CFF is satisfied (ie. CFF$\leq$ 0):

$$\text{CFF} = |F_\tau| + \mu_{fri} F_n - c \leq 0. \quad (3)$$

where μ_{fri} is the coefficient of friction and we consider various forms of slip weakening frictional laws for μ_{fri}, and c is a cohesive factor. We consider two different frictional laws for μ_{fri} in our numerical results: we consider a less strongly slip-weakening form where the mesh we use can resolve the underlying continuous system of equations for the continuous model, and a very strongly (highly non-linear) slip-weakening law for the discrete model.

To simulate multiple earthquake cycles we model different phases in the earthquake rupture separately to increase the speed and efficiency of our calculations. We implement a numerical method which consists of four distinct phases sequentially: tectonic loading to the next earthquake event, dynamic rupture of the fault, an absorbing wave phase, and a sub-cycle of any (dynamically determined) number of creep events between earthquakes. We emphasise that the method we use allows zero-velocity loading of the faults in contrast to many other numerical methods. Zero-velocity tectonic loading is appropriate for dynamic earthquake modelling because the tectonic strain rate is many orders of magnitude smaller than the transient strain rate due to seismic waves.

2 Single Fault Multicycle Dynamics

Previous studies of multicycle dynamics have shown strong mesh dependency of the numerical results. We consider two models in this section: a discrete model with very strongly slip-weakening friction (where the mesh size is too large to validly represent the underlying continuous system of equations), and a continuous system where less strongly slip-weakening friction is modelled. Rice (*JGR,1993*) first showed that models with oversized mesh elements, capable of failing independently of one another, may crudely represent geometrically disordered fault zones and mimic inherently discrete systems. Similarly to other studies we show that richly complex slip with a spectrum of event sizes can be reproduced with our discrete model. With mesh size reduction the spatio-temporally complex slip events disappear in favour of simple limit cycles of periodically repeated large earthquakes. Future work is underway into investigating if any models exist which can exhibit spatio-temporally complex slip at both large and small scales.

2.1 Continuous Model

Figure 1

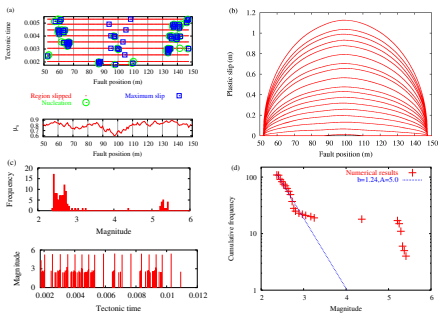

In the continuous regime only simple limit cycles of periodically repeating large earthquakes are observed. This could correspond to a long narrow individual fault, where a Gutenberg-Richter distribution of small events combined with enhanced statistics around a larger "characteristic" earthquake is observed naturally.

2.2 Discrete Model

Figure 2

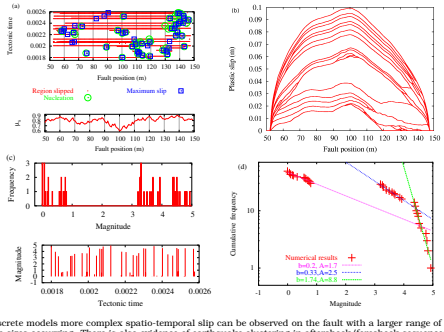

In discrete models more complex spatio-temporal slip can be observed on the fault with a larger range of earthquake sizes occurring. There is also evidence of earthquake clustering in aftershock/foreshock sequences. The effect of the static coefficient of friction is also much more evident in Figure 2(b) where the slip is larger towards the 50m fault end because the static coefficient of friction is on average lower (ie the fault is weaker) in this region. The static coefficient of friction along the fault is plotted in the bottom of Figure 2(a).

Slip time-histories along the fault in top of (a), static coefficient of friction along fault in bottom of (a) and the total slip accumulated after each event in (b). Frequency-size distribution of earthquakes in time in (c) and cumulative frequency-size distribution of earthquakes in (d). In (d) the data is fitted to $\log N(M) = A - bM$, where N is the cumulative frequency of earthquakes with magnitude greater than M and M is the magnitude. The magnitude (M) was calculated from the potency (P) where: $M = (2/3)\log P + 4.6$, and P is defined as: $P = \int_L \bar{u}(y)dy$, where L is the rupture length and $\bar{u}$ is the plastic slip. [Reference: *Zöller, Holschneider and Ben-Zion, PAGEOPH, 2005*]

3 Interacting Two-fault Systems

Earthquake triggering is the process by which stress changes associated with an earthquake can induce or retard seismic activity in the surrounding region. There is mounting evidence to suggest that small, sudden stress changes due to earthquakes can cause large changes in seismicity rates. Several kinds of earthquake interaction can affect seismicity rates. Calculations of static Coulomb stress (shear stress plus normal stress multiplied by the coefficient of friction) transfer have proven to be a powerful tool in explaining many near-field aftershock distributions (usually up to 1-2 fault lengths). Dynamic stress changes due to the passage of seismic waves cause transient dynamic stress oscillations, and in contrast, attenuate more slowly and thus dominate at large distances, depending on earthquake magnitude and directivity. Of the two mechanisms, dynamic triggering is the least understood. Generally seismologists can only attribute events occurring due to dynamic triggering based on distance from the fault or rupture directivity effects (as dynamic stress increases by an order of magnitude in the direction of rupture. In this section we consider interacting two-fault systems where both static and dynamic stress triggering are present.

3.1 Static Stress Triggering and Shadowing

3.1.1 Continuous Model

Figure 3

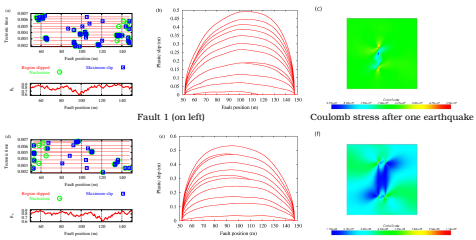

Fault 1 (on left) — Coulomb stress after one earthquake

Fault 2 (on right) — Coulomb stress after 84 earthquake events

Slip time-histories along fault 1 and 2 in (a) and (d) respectively, and total slip accumulated after each event for fault 1 and 2 in (b) and (e) respectively. The Coulomb stress after 1 earthquake event in (c), and after 84 events in (d), where fault 1 is on the left and fault 2 on the right.

Figures 3(b) and (d) both show evidence of static stress triggering at the ends $y = 150$m for fault 1 and $y = 50$m for fault 2 where larger slips occur towards these ends due to the positive Coulomb stress that accumulates at these ends during the earthquake cycle. Conversely at the opposite ends of both faults where the Coulomb stress is more negative, we see a general trend of smaller slips occurring at these ends due to stress shadowing. The resulting slip is no longer elliptical as in Figure 1(b).

The Coulomb stress is calculated by: Coulomb Stress= $|\sigma_\tau| + \mu_{\text{Sc}}\sigma_n$ where $\sigma_\tau = \boldsymbol{\sigma} \cdot \boldsymbol{n}^1 \cdot \boldsymbol{\tau}^1$, $\sigma_n = \boldsymbol{\sigma} \cdot \boldsymbol{n}^1 \cdot \boldsymbol{n}^1$ and $\mu_{\text{Sc}} = 0.9$. The faults are separated 20m from each other.

3.1.2 Discrete Model

Figure 4

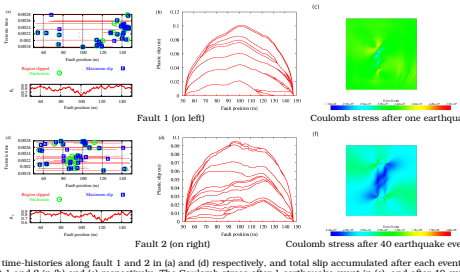

Fault 1 (on left) — Coulomb stress after one earthquake

Fault 2 (on right) — Coulomb stress after 40 earthquake events

Slip time-histories along fault 1 and 2 in (a) and (d) respectively, and total slip accumulated after each event for fault 1 and 2 in (b) and (e) respectively. The Coulomb stress after 1 earthquake event in (c), and after 40 events in (d), where fault 1 is on the left and fault 2 on the right.

Figures 4(b) and (d) also show evidence of static stress triggering and shadowing. However as we saw in Figure 2(b) when the discrete model was also used, the effect of the static coefficient of friction (shown in the bottom plot of (a) and (d)) is also important in determining when and where slip occurs.

The numerical results for fault 1 (where interactions with fault 2 are present) can be directly compared to the single fault case in Figure 2(a) and (b) as the same static coefficient of friction is defined on the fault. We can observe that the slip towards the end at 150m (where the Coulomb stress is positive) is greater in Figure 4(b) than Figure 2(b). Figure 4(a) also clearly shows that the earthquakes occurring on fault 2 lead to a suppression of earthquake activity on fault 1, especially towards the end at 50m (where the Coulomb stress is negative), compared to the single fault results in Figure 2(a).

3.2 Dynamic Stress Triggering

Figure 5

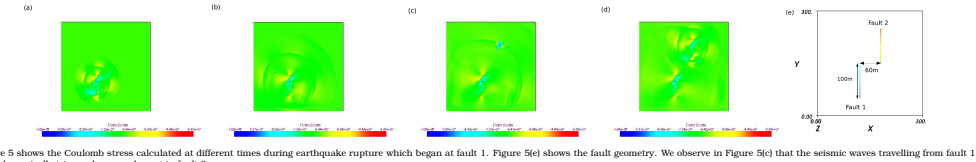

Figure 5 shows the Coulomb stress calculated at different times during earthquake rupture which began at fault 1. Figure 5(e) shows the fault geometry. We observe in Figure 5(c) that the seismic waves travelling from fault 1 have dynamically triggered a second event in fault 2.

Conclusions

We have verified that static stress shadowing and triggering, in addition to dynamic triggering have an effect on the observed seismicity in interacting fault systems in comparison to the background seismicity produced without earthquake interactions present. This is a feature which is difficult to study and prove in naturally occurring earthquake sequences.

ACKNOWLEDGEMENTS

This research is supported by the Australian Research Council Linkage project LP0562686 with the Queensland Department of Main Roads and the University of Queensland, and AuScope Ltd which is funded under the National Collaborative Research Infrastructure Strategy (NCRIS) an Australian Commonwealth Government Programme. Software was developed by the Australian Computational Earth Systems Simulator Major National Research Facility and computations were performed on the Australian Earth Systems Simulator, an SGI Altix 3700 supercomputer. I am grateful to Peter Mora for financial support.